OPTICAL INVESTIGATION OF LOW TEMPERATURE COMBUSTION AND SOOT EMISSION CHARACTERISTICS OF BIODIESEL/*n*-PENTANOL ENGINE

by

Song LI[a*], Jie SHI[a], Jinping LIU[b*], and Xianfu CHENG[a]

[a] School of Mechatronics and Vehicle Engineering,
East China Jiaotong University, Nanchang, China
[b] School of Mechanical Engineering, Anyang Institute of Technology, Anyang, China

Original scientific paper
https://doi.org/10.2298/TSCI240422179L

Biodiesel/n-pentanol blend fuels have been regarded as the attractive alternatives for the utilization of Diesel engines. However, the fundamental studies of low temperature combustion and soot formation characteristics of biodiesel/n-pentanol blend fuels in diesel engines are still scarce. The low temperature combustion and soot emission characteristics of pure waste cooking oil biodiesel (B100) and 70% waste cooking oil biodiesel/30% n-pentanol blend (B70P30) were experimentally studied in an optical engine in the present study. Results reveal that B70P30 has longer ignition delays than B100 at low exhaust gas re-circulation rate, but the ignition delays of B70P30 become similar or even shorter when the exhaust gas re-circulation rate is over 12%. Adding n-pentanol into biodiesel increases the in-cylinder combustion pressure peak and maximum pressure rise rate. In addition, the delay in the appearance of ignition kernels and two-color images are observed for B70P30 fuel. In the initial stage of fuel combustion, B70P30 has less ignition kernels and lower soot KL factor distribution area. In the middle and late stages of combustion, flame area of B70P30 is small and flame brightness is weaker. Also, at the end of combustion, the two-color images of B70P30 show that the soot KL factor distribution around the periphery of the chamber is decreasing at a higher rate compare to B100.

Key words: *optical engine, biodiesel, n-pentanol, low temperature combustion soot*

Introduction

Diesel engine serves as the main power source for agriculture, transportation and industry. However, fuel depletion and pollutant emission are fascinating researchers' attention developing advanced technologies to promote engine efficiency and reduce engine emissions [1]. Low temperature combustion (LTC) in Diesel engines has been recognized as one effective technology to concurrently decrease NO_x and particulate matter (PM) emission levels while maintaining high thermal efficiency. Exhaust gas re-circulation (EGR) coupling flexible fuel injection strategy can be used to achieve engine LTC mode [2]. However, a soot-bump region will arise with EGR increased despite it can be eliminated at high EGR operating conditions. Unfortunately, engine combustion efficiency will be deteriorated, and higher CO and unburned hydrocarbon (UHC) will be yielded at high EGR level [3]. Therefore, the utilization of alterna-

* Corresponding authors, e-mail: lisong57528@foxmail.com; liujinpinglucky@163.com

tive fuels and fuel additives to further improve efficiency and lower emissions of LTC Diesel engines has drawn a great deal of attention.

Biodiesel has emerged as a potential alternative fuel for Diesel engine application, which could be obtained from various resources, such as vegetable oils, waste cooking oils and animal fats [4]. It has several advantages, like high cetane number, better lubricity, carbon neutral, high oxygen content and mutual solubility with diesel [5]. Lower CO, UHC, PM, SO_2, and CO_2 emissions could be observed when Diesel engine using pure biodiesel or biodiesel/diesel [6]. However, several shortages are existed when Diesel engines fuelled with pure biodiesel, such as carbon deposits, piston ring sticking, oil-ways block and high NO_x emission, primarily owing to the high viscosity and poor volatility of biodiesel [5]. During the recent years, many researchers exhibited an increased interest in the optimization of biodiesel properties by blending additive into biodiesel to resolve those shortages.

Compared to biodiesel, renewable alcohols have lower viscosity and higher volatility also offer the additional oxygen content, which make it a promising blending component in enhancing the fuel properties of biodiesel fuel. As lower alcohols, methanol and ethanol have been widely used as fuel additives for biodiesel engines [7]. However, methanol and ethanol have phase separation at low temperatures and they have shown low engine performance and high emissions as well [8]. Compared to the lower alcohols, higher alcohols such as C4-butanol or C5-pentanol with longer carbon chains in their molecular structures have better miscibility with both diesel and biodiesel [9]. Also, higher alcohols provide higher cetane number, calorific value and lower latent heat of evaporation (LHE) compared with lower alcohols [10]. Thus, higher alcohols are regarded as better additives for biodiesel than lower alcohols.

As a higher alcohol, *n*-pentanol has been confirmed as a promising additive with biodiesel fuel. Zhang *et al.* [11] found that addition of *n*-butanol or *n*-pentanol to biodiesel produce higher brake specific fuel consumption (BSFC) but lower levels of PM and polycylic aromatic hydrocarbons. Zhu *et al.* [12] confirmed that adding *n*-pentanol into WCO biodiesel can obviously improve the combustion performance and decrease PM emission. But the blend fuels indicate an increase in CO and UHC emissions. Besides, adding 10% or 20% *n*-pentanol can decrease NO_x emission but the blend with 30% *n*-pentanol produces higher NO_x emission. In the paper of Yilmaz *et al.* [13], propanol, *n*-butanol and *n*-pentanol were added to WCO biodiesel, respectively. They observed that blend fuels reduce the brake thermal efficiency (BTE) except n-pentanol blend. Meanwhile, blending 10% *n*-pentanol with biodiesel can produce lower emission levels of CO, UHC, and NO_x while CO increased slightly at high engine load. According to Yilmaz *et al.* [14], biodiesel/*n*-pentanol binary fuels exhibited an increase in BTE. Compared to other biodiesel blends, adding 20% *n*-pentanol could reduce the emissions of CO, UHC, and NO_x under lower engine loads but increase these emissions at higher loads. Yang *et al.* [15] reported that when a direction-injection engine using biodiesel/*n*-pentanol blends, the number concentrations of PM emitted from Diesel engine can be decreased. Li *et al.* [5] concluded that adding *n*-pentanol into biodiesel leads to shorter spray penetration but greater spray cone angle due to the lower density and kinematic viscosity of *n*-pentanol. Ashok *et al.* [16] confirmed that the higher BTE can be achieved when *n*-pentanol is mixed with biodiesel up to 30%. While adding 40% *n*-pentanol into biodiesel deteriorates the engine performance and combustion. Additionally, biodiesel/*n*-pentanol blends can decrease CO, UHC, soot, and NO_x emission levels. Based on a constant volume combustion bomb, the spray and combustion processes of WCO biodiesel/*n*-pentanol blend fuels were evaluated by Ma *et al.* [17]. It was indicated that after blending *n*-pentanol, the spray and combustion characteristics are significantly improved, meanwhile the soot formation level is reduced.

Many studies have also proved that the *n*-pentanol can be employed as additive for biodiesel/diesel blends. Imdadul *et al.* [18, 19] concluded that the biodiesel/diesel/*n*-pentanol ternary blend fuels produce higher engine BTE and lower BSFC. The *n*-pentanol is more conducive to achieving higher BTE than *n*-butanol. In addition, ternary blends exhibit lower UHC and CO emissions but higher NO_x emission. However, another study [9] showed that biodiesel/diesel/*n*-pentanol ternary fuels have higher BSFC but lower BTE as compared to diesel fuel. In addition, higher emission levels of CO, UHC, and NO_x are produced by adding *n*-pentanol. Atmanli [20] revealed that adding *n*-pentanol to biodiesel/diesel binary blend can increase CO emission while decrease NO_x and UHC emissions. Dhanasekaran *et al.* [21] pointed out that compared to the biodiesel/diesel blend, higher BTE and lower BSFC are produced when Diesel engine using WCO biodiesel/diesel/*n*-pentanol ternary fuel. Also, CO, and smoke emissions are gradually reduced as the *n*-pentanol fraction increased. Huang *et al.* [22] found that biodiesel/diesel/*n*-pentanol ternary mixtures coupling EGR can effectively reduce UHC emission and improve the soot-NO_x trade-off relationship compared to diesel. Liang *et al.* [4] also observed that CO, UHC, and soot emission levels of biodiesel/diesel/*n*-pentanol mixtures are lower than pure diesel at larger EGR operating conditions, but NO_x emission keeps the same level with pure diesel.

As mentioned previously, *n*-pentanol has shown promise as an additive for pure biodiesel or biodiesel/diesel blend to enhance the fuel properties, however, very little research has been performed to explore the combustion of biodiesel/*n*-pentanol in LTC Diesel engine. Especially, previous researches have been intensely carried out on the all-metal Diesel engine, and the performance and exhaust pollutants are the main concerns. According to our knowledge, there is no experimental data of fundamental combustion and soot evolution processes for the biodiesel/*n*-pentanol engine under LTC mode up until now.

In the present work, the fundamental combustion and soot emission characteristics of WCO biodiesel/*n*-pentanol blend in LTC mode engine were experimentally explored and analyzed. Experiments were performed employing a modified direct injection four stroke single cylinder optical engine at different EGR rate conditions (0%~15%) with double injection strategy. Pure biodiesel and its mixture with 30% (by volume) of *n*-pentanol were evaluated. By using a color high speed camera, the development of in-cylinder combustion flame were captured. In addition, flame temperature and soot volume fraction distributions were derived and discussed from the combustion flame images.

Experiments

Engine specifications and instrumentations

Experimental investigation was accomplished using an optically accessible, direct injection, single cylinder, four stroke compression ignition engine with a detachable extended piston. Table 1 gives the optical engine specifications. Figure 1 illustrates the schematic diagram of the optical engine test set-up. As presented in fig. 1, an optical window made of full transparent quartz glass was installed on the piston crown using a metal ring. A 45° mirror that mounted below the optical piston was used to change the in-cylinder combustion flame light path, so that the combustion process could be recorded by the camera imaging system. Figure 2 represents the schematic view of the combustion chamber and view field for optical diagnostic. It can be observed that the flat optical piston can offer a 70 mm diameter field of view, which covers the injector and pressure sensor location. Besides, a 9-holes common rail diesel injector was placed at the center of the combustion chamber.

Table 1. Optical engine specifications

Parameter	Value
Number of cylinders	1
Valve type	DOHC 4 valves
Bore [mm]	96
Stroke [mm]	115
Geometric compression ratio	16.5
Piston type	flat
Fuel injection system	High pressure common-rail
Common rail injector	Bosch, 9 holes, equally spaced
Intake valve close [°CA bTDC]	155
Exhaust valve open [°CA aTDC]	155

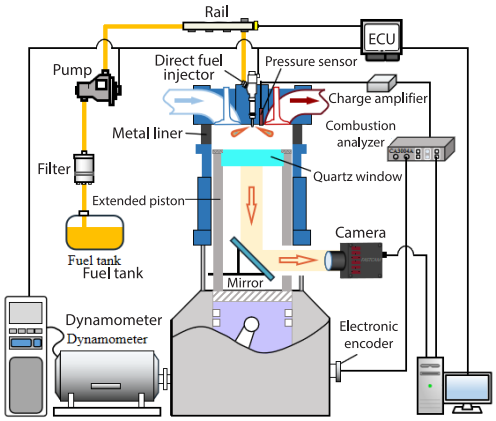

Figure 1. Schematic of the engine test system

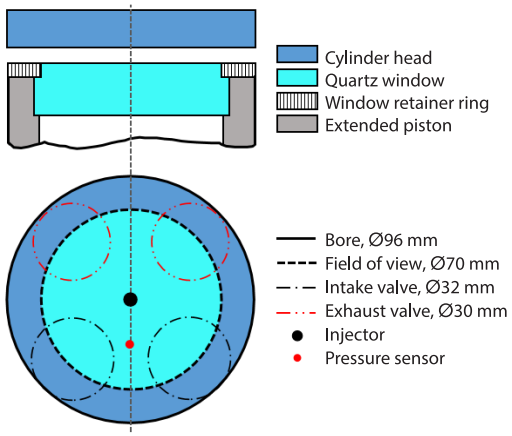

Figure 2. Schematic of the combustion chamber and view field for optical diagnostic

The test optical engine was motored by an eddy current dynamometer to control its speed. External regenerative air blower and electronic heater were equipped with the test engine to adjust the intake conditions. An open ECU control program was utilized to adjust the common-rail pressure, injection pulse width and injection timing. A color high speed camera (Photron FASTCAM Mini AX200) with a 105 mm f/2.8 Micro-Nikkor lens was used to catch the in-cylinder flame images. Synchronization of different control triggers for injection and camera could be accomplished by employing the same optical encoder installed on the engine crankshaft. A Kistler pressure transducer with a resolution of 0.1 °CA was employed to detect the in-cylinder pressure signals of the engine, the pressure transducer was fixed in the cylinder head, as shown in fig. 2. According to the First law of thermodynamics, the heat release rate (HRR) could be determined from the obtained in-cylinder pressure data.

Because CO_2 is the main component of real engine exhaust gas, also the dilution, thermal and chemical effects of EGR can be exerted by CO_2 on the engine combustion process [23], thus CO_2 was used to simulate EGR gas in the present study. The CO_2 was mixed with the intake air during the experiments, the proportion of CO_2 content in the intake gas was named

as EGR rate and it could be effectively adjusted by a EGR system. The EGR system consists of compressed CO_2 gas cylinder, relief valves and mass-flow controllers (MFC, with an accuracy of ±0.35% FS).

Test fuels

The WCO biodiesel and *n*-pentanol were used in the present study and tab. 2 gives the primary fuel properties. Considering that the proportion of *n*-pentanol addition into biodiesel was less than 30% in most of the investigations to reduce modification the engine systems [11-16]. Therefore, pure WCO biodiesel (referred to as B100) and WCO biodiesel (70%)/*n*-pentanol (30%) blend (on volume basis) (referred to as B70P30) were selected as two test fuels for the engine experiments. The B100 was presented for comparison. Solubility of B70P30 blend fuel was tested under 15 ℃ and no phase separation occurred.

Table 2. Properties of WCO biodiesel, *n*-pentanol and B70P30 [17, 24]

	WCO Biodiesel	*n*-pentanol
Molecular weight [kgkmol^{-1}]	~300	88.15
Cetane number	51	20
Oxygen content [wt.%]	11	18.15
Stoichiometric air/fuel ratio	11.3	11.7
Density at 20 °C [kgm^{-3}]	876	814.8
Kinematic viscosity at 40 °C [mm^{2}s^{-1}]	4.1	2.89
Low heating value [MJkg^{-1}]	37.5	35.1
Latent heating at 25 °C [kJkg^{-1}]	300	647.1
Heat capacity at 25 °C [MJkg^{-1}K^{-1}]	2.063	2.361
Boiling point [°C]	323 (T10) 329 (T50) 345 (T90)	138

Operating conditions

Experiments were carried out at a constant engine speed of 1000 rpm. The intake pressure was arranged at 1.1 bar. The intake temperature was heated to 80 °C. The total calorific value of B100 and B70P30 injected into the engine cylinder per cycle was kept the same (about 638J) and the common-rail pressure was controlled at 60 MPa. Considering the stiffness and strength of the quartz piston, double fuel injection strategy was utilized to lower cylinder pressure rise rate. The proportion of the two injections was 25%:75%, the first injection timing was 18 °CA bTDC, referred to as the pilot injection. The second injection was set at 6 °CA bTDC, referred to as the main injection. The EGR rate was changed from 0-15% with an interval of 3% during the test process. A summary of the engine operation conditions is listed in tab. 3. In addition, uniform camera exposure time and shooting rate were used during experiments to compare the combustion luminescence intensity of different test conditions. The came exposure time and image resolution were fixed to 20 μs and 512×512 pixels, respectively. The came frame rate was arranged to 10000 fps, thus the temporal resolution was 0.6 °CA at 1000 rpm engine speed.

Table 3. Engine operation conditions

Items	Value
Engine speed [rpm]	1000
Intake temperature [°C]	80
Intake pressure [bar]	1.1
Injection pressure [MPa]	60
1st injection [°CA bTDC]	–18
2nd injection [°CA bTDC]	–6
Ratio of 1st injection [%]	25
Ratio of 2nd injection [%]	75
EGR rate [%]	0~15

Flames images processing

The combustion flame brightness in Diesel engine can reflect the intensity of combustion in cylinder to a certain extent [25]. The flame luminescence intensity in each flame self-luminous image is defined as spatially integrated natural luminosity (SINL) [26]. The color of the self-luminous image is determined according to the three RGB values in each pixel. In this work, a MATLAB program was used to extract the RGB values of all pixels in the image, then the RGB values were superimposed to obtain the SINL value. The calculation formula is: $Y = 0.299R + 0.587G + 0.114B$. The Y is the brightness of the whole combustion image in the formula, that is, the value of SINL, R, G, and B represent the chrominance components of RGB three primary colors captured by the high speed camera, respectively.

For further analyze the combustion flame, the self-luminous flame image was further processed and analyzed by the two-color method [27, 28] to acquire the information of 2-D flame temperature and soot concentration fields. The relative soot volume concentration in the combustion flame is characterized by the KL factor. Based on the theory of solid thermal radiation, the two-color method has high time resolution [25] and the detailed principle can be seen in the literature [27, 28]. Before the experiment, the high speed camera was calibrated by the blackbody furnace calibration test, and the curve relationships between different temperature, aperture and exposure time and flame image radiation intensity were established.

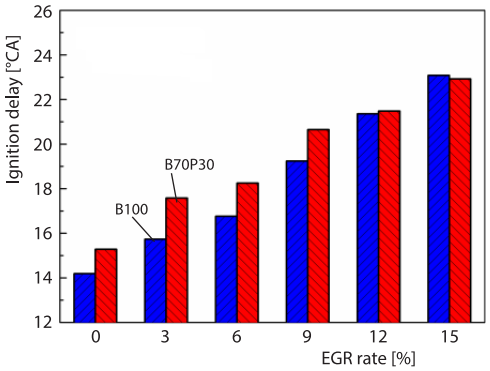

Figure 3. The IDT of B100 and B70P30

Result and discussions

Combustion characteristics

Figure 3 depicts the ignition delay times (IDT) of B100, and B70P30 at different EGR rates. As shown, the IDT for B100 and B70P30 fuels are prolonged with increasing the EGR rate, the IDT retard 8.9 °CA and 7.6 °CA for B100 and B70P30, respectively when EGR changed from 0-15%. This trend could result from the thermal and diluent effects of dilution gas [4]. The in-cylinder temperature will be decreased with the addition of CO_2 into the intake air due to CO_2 has higher specific heat capacity

compared to air [29]. Besides, the local oxygen concentration will be decreased caused by the diluent effect of CO_2, which decreases the effective collision frequency between fuel and O_2, prolonging the chemical preparation process.

It can also be observed that B70P30 obviously exists longer IDT than B100 under the low EGR regime (below 9%). Huang *et al.* [30] confirmed that the fuel properties, such as cetane number, LHE, and auto-ignition temperature, have a great influence on the IDT. As shown in tab. 2, *n*-pentanol has lower cetane number value than that of biodiesel, thus adding *n*-pentanol leads to longer chemical delay period. Meanwhile, *n*-pentanol has higher LHE and heat capacity as compared to biodiesel, which can exert a cooling effect on the fuel/air mixture temperature. However, when the EGR rate is increased exceeds 9%, it is worth to be noted that the over-delayed ignition problem is relieved, B70P30 has similar and even shorter IDT compared to B100. The result is similar to those reported in the previous works [4, 17]. Ma *et al.* [17] pointed out that this behavior may be caused by the different dependence of ignition reactivity on environment temperature and oxygen concentration between biodiesel and *n*-pentanol.

Figure 4 gives the in-cylinder pressure and HRR curves under various EGR rates for B100 and B70P30. As seen, the combustion pressure and HRR profiles of B100 and B70P30 show two-stage combustion pattern according to the number of injections at low EGR rate. Another observation is that the pressure and ROHR curves are sensitive to the variation of EGR. As the EGR increased, the HRR curves of the two fuels gradually transition from two-stage heat release to single-stage heat release, the in-cylinder combustion pressure curves show a downward trend and the first-stage combustion is no longer obvious as EGR rate greater than 12%. The first heat release peak gradually decreases while the second HRR peak continues to rise until the EGR rate reaches 15%, and the phase of peak HRR continues to retard.

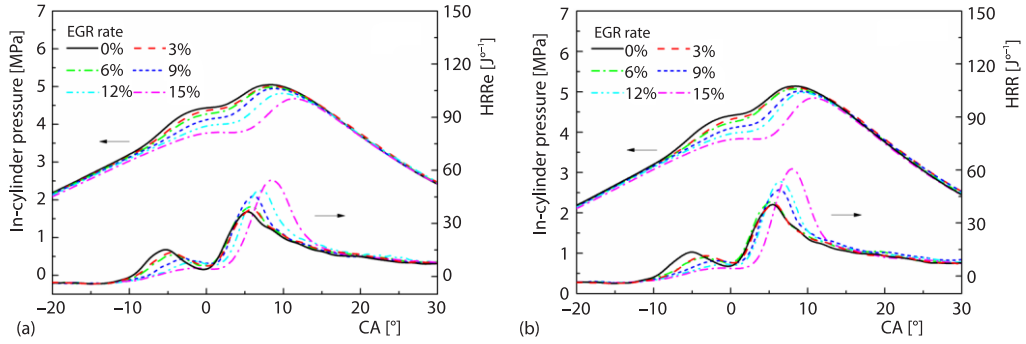

Figure 4. In-cylinder pressures and HRR of B100 and B70P30; (a) B100 and (b) B70P30

As the EGR increased from 0-15%, the ignition performance of the early pilot fuel is weakened owing to the thermal and diluent effects of CO_2, more pilot injected fuel cannot be completely burned, so the first stage heat release caused by pilot injection fuel is gradually delayed and weakened. The deterioration of first injection fuel combustion gives rise to the lower in-cylinder temperature and pressure, and the longer IDT of the main injection fuel. Longer IDT facilitates uniform mixing of combustion mixture. Besides, the reactivity of in-cylinder mixture can be improved by the premixing of unburned pilot injected fuel. Therefore, the second stage heat release is gradually enhanced. The peak in-cylinder pressure decreases steadily can be explained by the inhibition of first injection fuel combustion and the ignition time of second injection fuel occurs more far away from TDC. When EGR changes from 0% to15%, the peak pressures are decreased by 7.29% and 5.66% for B100 and B70P30, respectively, but the second HRR peak values are increased by 48.78% for B100 and 50.15% for B70P30.

Figure 5 displays the in-cylinder pressures and HRR of two fuels at 0%, 6%, 12%, and 15% EGR. Adding *n*-pentanol to biodiesel fuel results in lower first HRR peaks and higher second HRR peaks. Additionally, the combustion pressure peaks are increased, the corresponding increase in combustion pressure peaks are 1.78%, 1.77%, 3.43%, and 3.57% compared to D100 at 0%, 6%, 12%, and 15% EGR, respectively. This phenomenon is the result of the synergistic effect of the difference of physicochemical properties between biodiesel and *n*-pentanol. The B70P30 fuel yields better fuel spray atomization and evaporation than B100 due to the lower viscosity, density and higher volatility of *n*-pentanol. Also, although the ignition and combustion behaviors of pilot injected B70P30 are inhibited because of the cooling effect of evaporation process, the premixing of unburned B70P30 fuel is beneficial to improve the premixed combustion of main injected fuel. Additionally, B70P30 fuel has more oxygen content. All those factors are conducive to promoting the engine combustion process and increasing the peaks of combustion pressure and second stage heat release for B70P30.

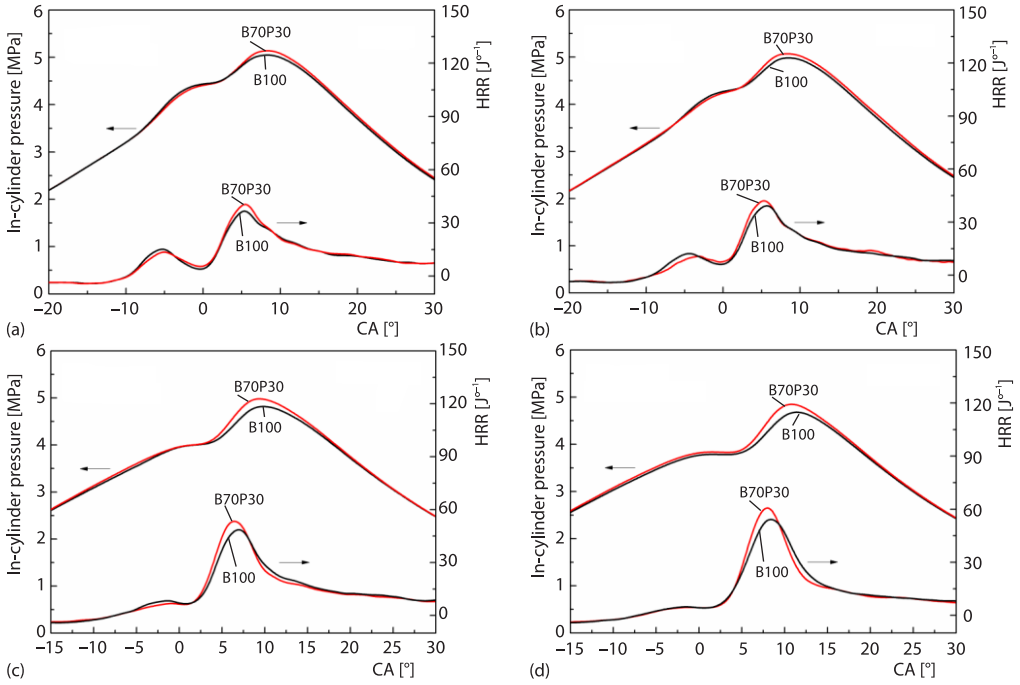

Figure 5. In-cylinder pressures and HRR of B100 and B70P30 at different EGR rates; (a) 0% EGR, (b) 6% EGR, (c) 12% EGR, and (d) 15% EGR

Figure 6 indicates the behaviors of the pressure rise rates for B100 and B70P30 under various EGR conditions. As shown in figs. 6(a) and 6(b), the variation of pressure rise rate curves as increasing EGR rate is consistent with the behavior of HRR. In addition, it is clear that the maximum values of pressure rise rate curves (MPRR) of B100 and B70P30 first decrease and then increase with increasing the EGR rate, see fig.6(c). Compared to B100, B70P30 has similar or even lower MPRR value at low EGR rate. That is because that the MPRR is dominated by the first heat release at low EGR conditions but the heat release of pilot injected B70P30 is weakened due to its higher LHE and heat capacity. However, a marked increase in MPRR values is found for B70P30 when the EGR rate exceeds 6%, which can be mainly ascribed to that B70P30 has higher proportion of premixed combustion regime.

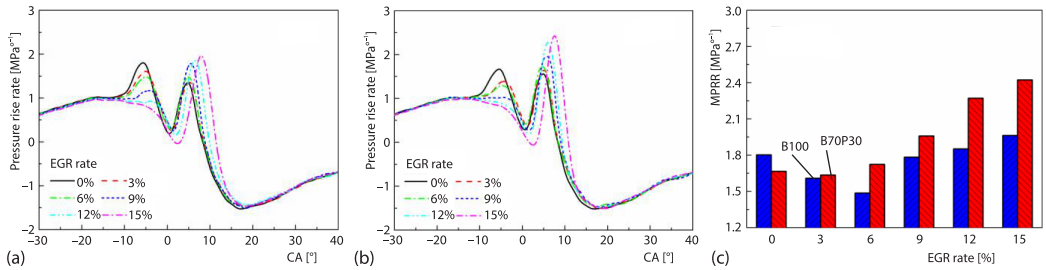

Figure 6. Pressure rise rates of B100 and B70P30; (a) B100, (b) B70P30, and (c) MPRR

Flame development imaging

Figures 7-9 present the true-color combustion images of the two fuels. For the sake of brevity, 12 images are selected to represent the whole combustion process and only three test conditions (0%, 9%, and 15% EGR) are chosen to present here. The white circles in the images denote the optical window boundary. As shown in fig.7(a), for B100 fuel, at 0% EGR condition, the ignition kernels of the pilot injection fuel are formed in the spray envelope near the downstream edge of the spray at –7 °CA aTDC. After that, more flame kernels emerge successively and merge with each other. At 1.4 °CA aTDC, a part of the main injected biodiesel is ignited without atomization owing to the heat release of the pilot injected fuel, so some bright diffusion flames appear at the center of the combustion chamber. As shown, these bright flames are developing along the injection direction in the period between 2.6 °CA-3.8 °CA aTDC. At 5 °CA aTDC, the bright flames have high light intensity and saturate the camera signal, also the whole optical window is almost flooded with those bright flames. The combustion luminosity primarily comes from soot incandescence in the locally fuel rich zones [31]. From 11 °CA aTDC, a later stage of combustion proceeds with decreasing combustion luminosity and flame area. In the period between 14 °CA-44 °CA aTDC, the combustion flame remains near the vicinity of the optical window in the direction of fuel injection,

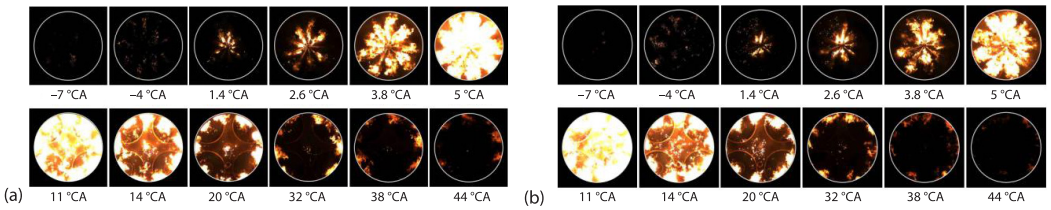

Figure 7. Flame development images of B100 and B70P30 with 0%EGR rate [aTDC]; (a) B100 and (b) B70P30

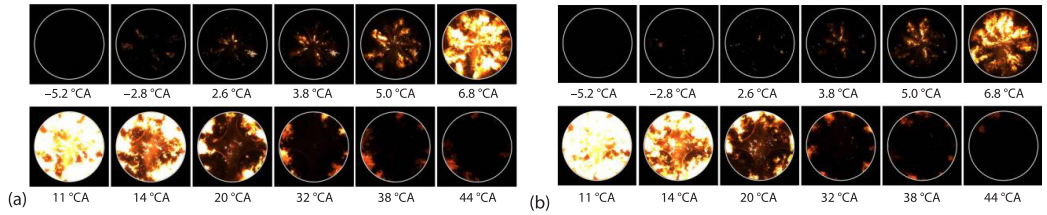

Figure 8. Flame development images of B100 and B70P30 with 9%EGR rate [aTDC]; (a) B100 and (b) B70P30

this trend can be possibly due to the centrifugal force generated by in-cylinder swirl flow and the lower density of the high temperature burned gases. The flame development behaviors of B70P30 are similar to those of B100 fuel. But compared to B100 fuel, B70P30 has less ignition kernels at the beginning of combustion. In the middle and late stages of combustion, the flame area of B70P30 is small, and the flame brightness is weaker, this is possibly because that the formation of soot particle can be reduced by blending *n*-pentanol to biodiesel.

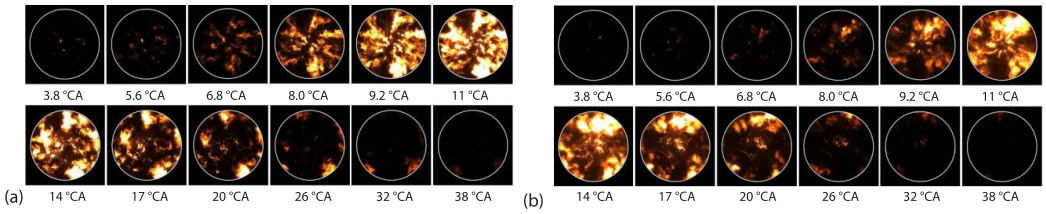

Figure 9. Flame development images of B100 and B70P30 with 15% EGR rate [aTDC]; (a) B100 and (b) B70P30

It can be seen in figs. 7-9 that an increase of the EGR rate results in a marked delay in the appearance of the B100 and B70P30 combustion images, particularly, the fuel ignition starts in the process of main fuel injection at 15% EGR, which is consistent with the ignition delays of fig. 3. Meanwhile, as increasing EGR rate, the flame luminosity of combustion images is significantly decreased. Figure 10 depicts the SINLvalues of B100 and B70P30. As seen, when EGR rate changes from 0% to 15%, the peak values of SINL curves are reduced by 47.84% for B100 and 48.37% for B70P30. In addition, flame propagation behaviors show that flame structure becomes more discrete and more irregular as increasing EGR rate. Without EGR, it can be obviously found that the shape of the flame distribution strongly resembles that of the fuel spray at early phase of combustion, while at 15% EGR, the shape of the flame seems to have no obvious relationship with the fuel spray. Those phenomena can be explained that CO_2 is an inert gas with a larger specific calorific value, adding CO_2 to the intake air will slow down the pre-flame reaction and hinder the flame propagation. Also, it will reduce the intake volume of air, resulting in lower in-cylinder oxygen content and lower air-fuel ratio. Therefore, the ignition time of fuel is delayed, the flame propagation is hindered, and the combustion intensity and flame brightness are significantly reduced.

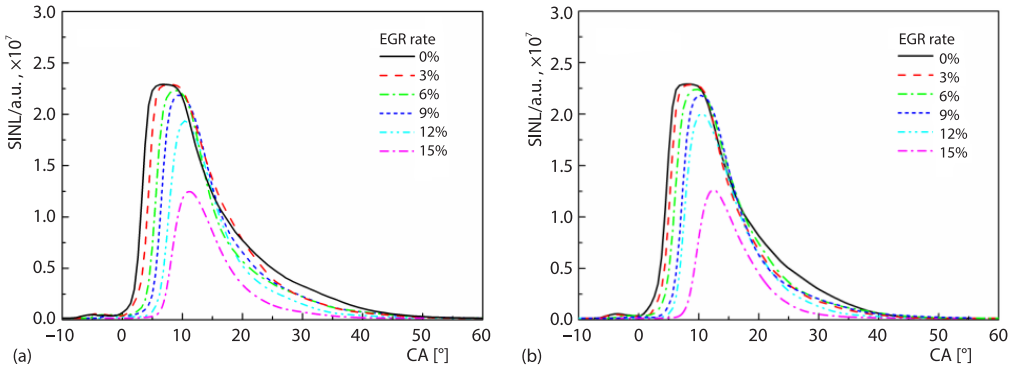

Figure 10. Flame SINL values of B100 and B70P30; (a) B100 and (b) B70P30

Soot temperature and volume fraction

Figures 11-13 show the soot temperature and KL factor evolutions of B100 and B70P30 at selected CA for 0%, 9%, and 15% EGR conditions. At 0% EGR rate, at the beginning of fuel combustion, it can be observed in fig. 11 that few high temperature and soot KL factor zones appear. After then, the bright diffusion flame develops rapidly, so the distribution areas of soot temperature and KL factor increase rapidly. Because the luminescence and heat release of combustion are occurred concurrently, so the high temperature areas mainly appear in the luminous zones that are assembled and distributed in the fuel injection direction, see fig. 7. Soot KL factors gradually increase and are mainly concentrated near the center of the flame luminous zones, this area belongs to the rich burning area with rich fuel and little oxygen, which is beneficial to the soot formation. But the soot KL factors at the outer edge of the flame are low because of the air-fuel ratio at those regions is larger, which is conducive to the soot oxidation process. Towards the middle to late of combustion, as the piston moves downward, it can be observed that the images show a decrease in the spatial distribution areas of soot temperature and KL factor.

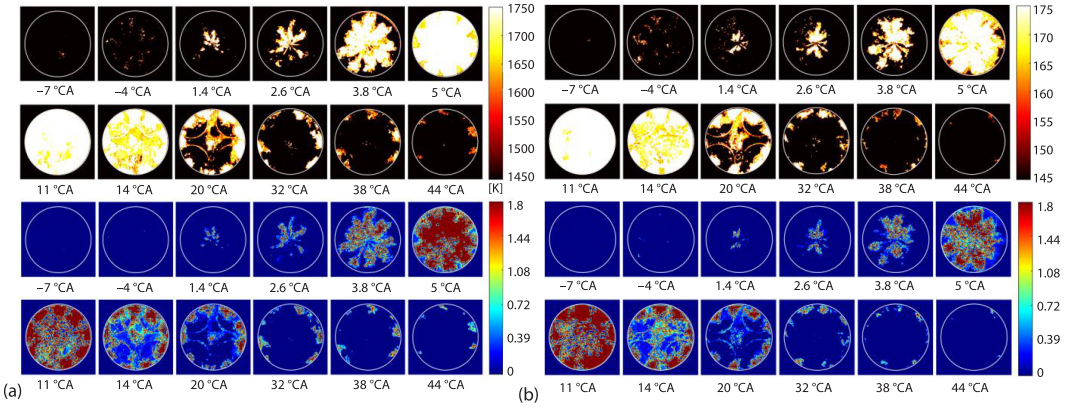

Figure 11. Soot temperature and KL factor images of B100 and B70P30 with 0% EGR rate [aTDC]; (a) B100 and (b) B70P30

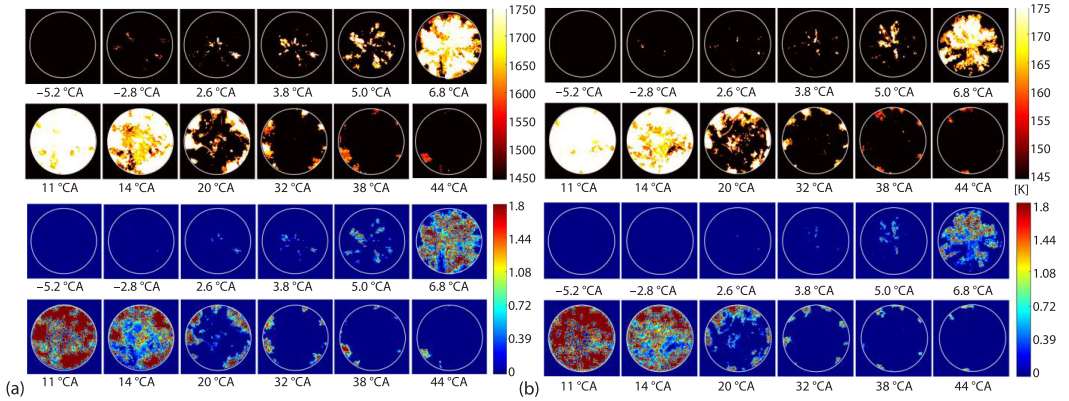

Figure 12. Soot temperature and KL factor images of B100 and B70P30 with 9% EGR rate [aTDC]; (a) B100 and (b) B70P30

Combined with figs. 11-13, the distributions of soot temperature and KL factor are obviously effected by EGR. An increase of EGR obviously delays the appearance of soot particle and reduces the distribution fields, which meas the soot formation process is inhibited. In addition, the soot temperature and KL factor evolution processes of B70P30 are similar to those of B100 fuel at different EGR conditions. However, compared to B100, B70P30 has lower distribution areas of soot temperature and KL factor in the initial stage of combustion. Also, the images of B70P30 show that their soot KL factor distribution around the periphery of the chamber is decreasing at a higher rate in comparison B100 at the late of combustion.

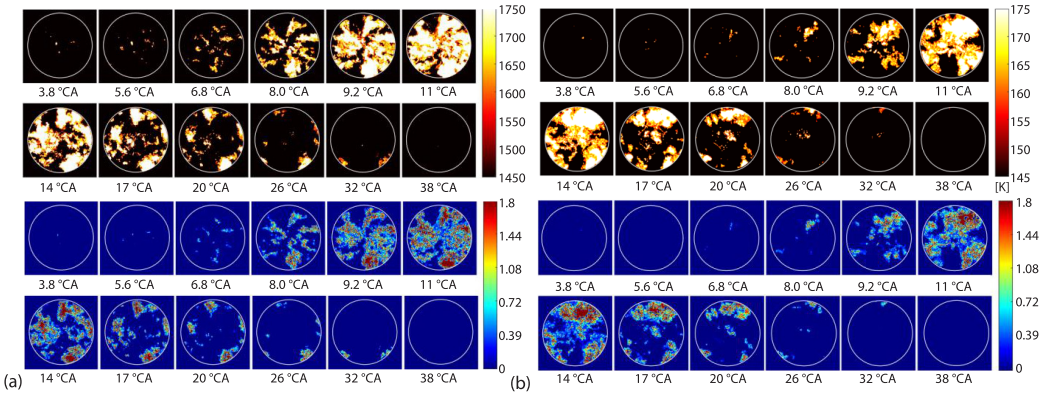

Figure 13. Soot temperature and KL factor images of B100 and B70P30 with 15% EGR rate [aTDC]; (a) B100 and (b) B70P30

For more quantitative analysis, the soot temperature and KL factor distribution cumulative histograms of B100 and B70P30 under the three EGR rates (0%, 9%, and 15%) are described in fig. 14, respectively. As shown, at 0% EGR, a small number of low temperature (1450 K < $T \leq$ 1750 K) and soot KL factor (0 < KL factor $\leq$ 0.5) regions appear at –7.5 ~ –2.5 °CA aTDC. But in the period between 2.5 °CA and 15 °CA aTDC, a large number of high soot temperature (1850 K < $T \leq$ 1950 K) and KL factor (KL > 1.5) appears and increases greatly. This is mainly attributed to the main injected fuel is ignited without atomization, leading to a large number of diffusion flame. The soot temperature and *KL* factor distributions gradually decrease in the late combustion stage, but the proportions of low temperature and soot KL factor are greatly increased. Additionally, it can be observed that the shapes of the distribution curves of soot temperature and KL factor (0 < KL factor $\leq$ 1.5) show bimodal structure for B100 and B70P30 at 0% EGR rate, the high soot temperature (T > 1950 K) distribution is concentrated at two peaks. This is because the combustion process presents a two-stage combustion without EGR.

With increasing the EGR rate, the area curves of soot temperature and KL factor distribution regions changes to unimodal structure. The values of soot temperature and KL factor in each region are reduced, also the crossed crankshaft angle decreases obviously. Also, the proportions of high flame temperature (1850 K < $T \leq$ 1950 K and T > 1950 K) and soot KL factor (KL > 1.5) are decreased significantly. Particularly, the low temperature (1450 K < $T \leq$ 1850 K) and soot KL factor (0 < KL factor $\leq$ 1.0) zones dominate the whole combustion process at 15% EGR. Therefore, adding CO_2 to the engine intake air can change the in-cylinder temperature field distribution, reduce the high combustion temperature and narrow the temperature gradient, which contribute to the realization of low temperature homogeneous combustion. The addition of CO_2 produce lower soot KL factor can be explained:

– The dilution and thermal effects of CO_2 results in longer IDT, which can have a beneficial to reduce fuel-rich and high temperature zones, thereby inhibiting the soot formation.
– The chemical effect of CO_2 can reduce the rates of soot inception, surface growth by acetylene addition and pyrene condensation [32]. The OH produced by chemical reaction of CO_2 at high temperature, *i.e.* $CO_2 + H \leftrightarrow CO + OH$, can enhance the oxidation process of both soot precursor and soot particle [32].
– The CO_2 can increase the soot surface oxidation activity [23]. As a consequence, the oxidation reactions between soot and the surrounding O_2, OH, *etc*. are promoted. The CO_2 can also react directly with soot particles ($CO_2 + C \rightarrow 2CO$), thereby decreasing soot particles formation [33].

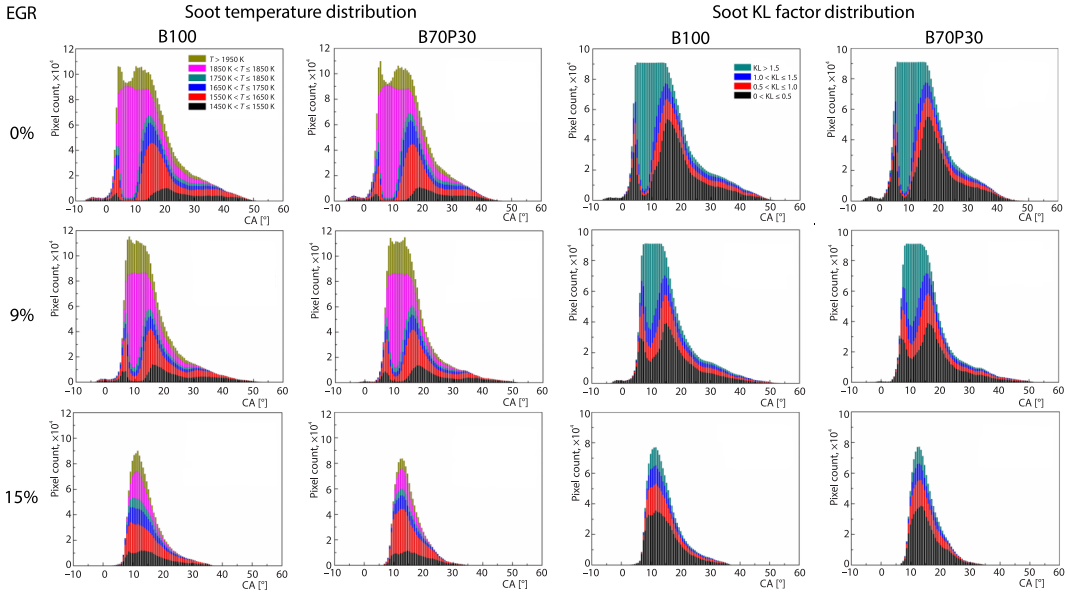

Figure 14. Soot temperature and KL factor distributions at 0%, 9%, and 15% EGR rates

The B70P30 has similar flame temperature and KL factor distributions with those of B100, but the crossed crankshaft angle of the distributions for B70P30 decreases obviously. In particularly, B100 and B70P30 have a similar ignition timing at 15% EGR, but the flame temperature and KL factor distributions of B100 mainly concentrate in the period between 5-37 °CA aTDC, and the these areas of B70P30 are concentrated between 7-32 °CA aTDC, which implies the soot formation rate is decreased while the oxidation rate is enhanced by blending *n*-pentanol into biodiesel. It can be explained by several primary reasons. First, B70P30 has better fuel spray atomization characteristic due to the lower viscosity and higher volatility of *n*-pentanol, which is favorable to generate a more homogeneous fuel-air mixture [4, 34]. Second, *n*-pentanol has less carbon atom and aromatics contents compared to biodiesel, so the formation of soot precursors and soot can be prevented [35]. Third, the oxygen atoms offered by *n*-pentanol can evidently lessen the local fuel rich region, improve the combustion process and promote the oxidation processes of soot precursor and soot particle [36]. Fourth, *n*-pentanol can yield more small radicals at the initial stage of high temperature combustion [4], which can oxidize carbon atom to CO and CO_2 and restrain the formation of soot precursors.

Conclusions

The combustion and soot emission characteristics of B100 and B70P30 were fundamental studied under the simulated EGR conditions in this study on an optical engine with double injection strategy. The flame development processes of two fuels were recorded employing a Photron camera. The information of soot temperature and KL factor distributions was obtained from the combustion phase images by using the two-color method. The following conclusions were summarized based on the obtained in-cylinder data and combustion images, are as follows.

– With increasing the EGR rate, the ignition timing periods for B100 and B70P30 fuels are prolonged, the in-cylinder pressure peaks are decreased and their phase positions are delayed, the two-stage heat release evolves into single-stage heat release with higher HRR peak value, the MPRR values first decrease and then increase.
– Compared to B100, B70P30 obviously exists longer IDT than B100 when the EGR rate smaller than 9%, while B70P30 has a similar or even shorter IDT than B100 at high EGR rates. Meanwhile, adding *n*-pentanol to biodiesel fuel results in higher combustion pressure peak and MPRR values.
– High EGR rates significantly delay the appearance of ignition kernel, disperse the flame structure, and decrease the flame area and luminosity. In addition, high EGR rates can reduce the distribution areas of the soot temperature and KL factor, reduce the average combustion temperature and narrow the temperature gradient, decrease the soot KL factor values in each region.
– The B100 and B70P30 perform similar flame development and soot formation behaviors. But compare to B100 fuel, B70P30 has less ignition kernels at early stage of combustion, weaker flame brightness and smaller flame area. Also, the crossed crankshaft angles of the soot temperature and KL factor distributions of B70P30 decrease obviously, which means the soot formation is inhibited by adding *n*-pentanol into biodiesel.

Acknowledgment

This work was supported by the Key R&D and Promotion in Henan Province Special Project (232102220087).

References

[1] Paykani, A., *et al*., Reactivity Controlled Compression Ignition Engine: Pathways Towards Commercial Viability, *Applied Energy*, *282* (2021), 116174
[2] Huang, H. Z., et al., Comparative Study of Effects of Pilot Injection and Fuel Properties on Low Temperature Combustion in Diesel Engine under a Medium EGR Rate, *Applied Energy*, *179* (2016), Oct., pp. 1194-1208
[3] Zheng, Z. Q., *et al*., Experimental Study on the Combustion and Emissions Fueling Biodiesel/N-Butanol, Biodiesel/Ethanol and Biodiesel/2,5-Dimethylfuran on a Diesel Engine, *Energy*, *115* (2016), Part 1, pp. 539-549
[4] Liang, J., *et al*., The Effects of EGR Rates and Ternary Blends of Biodiesel/n-Pentanol/Diesel on the Combustion and Emission Characteristics of a CRDI Diesel Engine, *Fuel*, *286* (2021), 119297
[5] Li, F., *et al*., Comparison of Macroscopic Spray Characteristics between Biodiesel-Pentanol Blends and Diesel, *Experimental Thermal and Fluid Science*, *98* (2018), Nov., pp. 523-533
[6] Thiyagarajana, S., *et al*., Effect of Manifold Injection of Methanol/N-Pentanol in Safflower Biodiesel Fuelled CI Engine, *Fuel*, *261* (2020), 116378
[7] Niculescu, R., *et al.*, Review on the Use of Diesel-Biodiesel-Alcohol Blends in Compression Ignition Engines, *Energies*, *12* (2019), 1194
[8] Babu, D., Anand R., Effect of Biodiesel-Diesel-N-Pentanol and Biodiesel-Diesel-Nhexanol Blends on Diesel Engine Emission and Combustion Characteristics, *Energy*, *133* (2017), 15, pp. 761-776

[9] Yilmaz, N., Atmanli A., Experimental Assessment of a Diesel Engine Fueled with Diesel-Biodiesel-1-Pentanol Blends, *Fuel*, *191* (2017), Mar., pp. 190-197
[10] Coughlin, B., Hoxie A., Combustion Characteristics of Ternary Fuel Blends: Pentanol, Butanol and Vegetable Oil, *Fuel*, *196* (2017), May, pp. 488-496
[11] Zhang, Z. H., Balasubramanian, R., Investigation of Particulate Emission Characteristics of a Diesel Engine Fueled with Higher Alcohols/Biodiesel Blends, *Applied Energy*, *163* (2016), Feb., pp. 71-80
[12] Zhu, L., *et al*., Combustion, Gaseous and Particulate Emission of a Diesel Engine Fueled with n-Pentanol (C5 Alcohol) Blended with Waste Cooking Oil Biodiesel, *Applied Thermal Engineering*, *5* (2016), June, pp. 73-79
[13] Yilmaz, N., *et al*., Performance of Biodiesel/Higher Alcohols Blends in a Diesel Engine, *International Journal Energy Research*, *40* (2016), 8, pp. 1134-1143
[14] Yilmaz, N., *et al.*, Influence of 1-Pentanol Additive on the Performance of a Diesel Engine Fueled with Waste Oil Methyl Ester and Diesel Fuel, *Fuel*, *207* (2017), Nov., pp. 461-469
[15] Yang, K., *et al*., The Effect of Pentanol Addition on the Particulate Emission Characteristics of a Biodiesel Operated Diesel Engine, *Fuel*, *209* (2017), Dec., pp. 132-140
[16] Ashok, B., *et al.*, An Experimental Analysis on the Effect of n-Pentanol-Calophyllum Inophyllum Biodiesel Binary Blends in CI engine Characteristcis, *Energy*, *173* (2019), Apr., pp. 290-305
[17] Ma, Y., *et al.*, Experimental Investigation on the Effect of N-Pentanol Blending on Spray, Ignition and Combustion Characteristics of Waste Cooking Oil Biodiesel, *Energy Conversion and Management*, *148* (2017), Sept., pp. 440-455
[18] Imdadul, H. K., *et al.*, A Comparative Study of C4 and C5 Alcohol Treated Diesel-Biodiesel Blends in Terms of Diesel Engine Performance and Exhaust Emission, *Fuel*, *179* (2016), Sept., pp. 281-288
[19] Imdadul, H. K., *et al.*, Higher Alcohol-Biodiesel-Diesel Blends: An Approach for Improving the Performance, Emission, and Combustion of a Light-Duty Diesel Engine, *Energy Conversion and Management*, *111* (2016), Mar., pp. 174-185
[20] Atmanli, A., Comparative Analyses of Diesel-Waste Oil Biodiesel and Propanol, n-Butanol or 1-Pentanol Blends in a Diesel Engine, *Fuel*, *176* (2016), 15, pp. 209-215
[21] Dhanasekaran, R., *et al*., A Sustainable and Eco-Friendly Fueling Approach for Direct-Injection Diesel Engines Using Restaurant Yellow Grease and n-Pentanol in Blends with Diesel Fuel, *Fuel*, *1* (2017), 193, pp. 419-431
[22] Huang, H., *et al*., Assessment of n-Pentanol Additive and EGR rates Effects on Spray Characteristics, Energy Distribution and Engine Performance, *Energy Conversion and Management*, *202* (2019), 112210
[23] Zhang, W., *et al*., Properties and Oxidation of in-Cylinder Soot Associated with Exhaust Gas Re-Circulation (EGR) in Diesel Engines, *Proceedings of the Combustion Institute*, *38* (2020), 1, pp. 1319-1326
[24] Sarathy, S. M., *et al*., Alcohol Combustion Chemistry, *Progress in Energy and Combustion Science*, *44* (2014), Oct., pp. 40-102
[25] Liu, H. F., *et al*., Comparison of Ethanol and But*an*ol as Additives in Soybean Biodiesel Using a Constant Volume Combustion Chamber, *Energy and Fuels*, *25* (2011), 4, pp. 1837-1846
[26] Yang, C., *et al*., Experimental Study On The Interactions of Wall Temperature and Impingement Distances and Their Effects on the Impinged Diesel Spray Ignition and Combustion Characteristics, *Applied Thermal Engineering*, *230* (2023), 120670
[27] Zhao, H., Ladommatos, N., Optical Diagnostics for Soot and Temperature Measurement in Diesel Engines, *Progress in Energy and Combustion Science*, *24* (1998), 3, pp. 221-255
[28] Payri, R., *et al*., Measurement of Soot Concentration in a Prototype Multi-Hole Diesel Injector by High-Speed Color Diffused Back Illumination Technique, SAE Technical Paper, 2017-01-2255, 2017
[29] Li, W. F., *et al.*, Experimental and Theoretical Analysis of Effects of Atomic, Diatomic and Polyatomic Inert Gases in Air and EGR on Mixture Properties, Combustion, Thermal Efficiency and NO_x Emissions of a Pilot-Ignited NG engine, *Energy Conversion and Management*, *105* (2015), Nov., pp. 1082-1095
[30] Huang, H. Z., *et al.*, An Experimental Study on the Combustion and Emission Characteristics of a Diesel Engine under Low Temperature Combustion of Diesel/Gasoline/n-Butanol Blends, *Applied Energy*, *170* (2016), May, pp. 219-231
[31] Payri, F., *et al*., Contribution the Application of Two-Color Imaging to Diesel Combustion, *Measurement Science and Technology*, *18* (2007), 2579
[32] Liu, F., *et al*., Numerical and Experimental Study of the Influence of CO_2 and N_2 Dilution on Soot Formation in Laminar Coflow C_2H_4/Air Diffusion Flames at Pressures Between 5 and 20 ATM, *Combustion and Flame*, *162* (2015), 5, pp. 2231-2247

[33] Zhang, Q. C., *et al.*, Experimental and Simulation on Diesel Low Temperature Combustion of Charge Compositions, *Transactions of CSICE*, *29* (2011), 6, pp. 481-488
[34] Feng, Z. H., *et al.*, Experimental Investigation on Spray and Atomization Characteristics of Diesel-Gasoline-Ethanol Blends in High Pressure Common Rail Injection System, *Energy*, *112* (2016), Oct., pp. 549-561
[35] Nabi, M. N., Hustad, J. E., Influence of Oxygenates on Fine Particle and Regulated Emissions from a Diesel Engine, *Fuel*, *93* (2012), Mar., pp. 181-188
[36] Tan, P. Q., *et al*., Particle Number and Size Distribution from a Diesel Engine with Jatropha Biodiesel Fuel, SAE Technical Paper, 2009-01-2726, 2009

Paper submitted: April 22, 2024
Paper revised: May 19, 2024
Paper accepted: May 23, 2024

2024 Published by the Vinča Institute of Nuclear Sciences, Belgrade, Serbia.
This is an open access article distributed under the CC BY-NC-ND 4.0 terms and conditions